Journal of Alloys and Compounds 756 (2018) 26–32

Contents lists available at ScienceDirect

Journal of Alloys and Compounds

journal homepage: http://www.elsevier.com/locate/jalcom

Structures and mechanical properties of Nb-Mo-Co(Ru) solid solutions for hydrogen permeation

Fei Liu [a, c], Zejun Xu [b], Zhongmin Wang [b, **], Mengyao Dong [d, e], Jianqiu Deng [b], Qingrong Yao [b, ***], Huaiying Zhou [b], Yong Ma [d, h], Jiaoxia Zhang [e, f], Ning Wang [g], Zhanhu Guo [e, *]

[a] Department of Materials Engineering, Taiyuan Institute of Technology, Taiyuan 030008, China
[b] School of Material Science and Engineering, Guilin University of Electronic Technology, Guilin 541004, China
[c] School of Material Science and Engineering, North University of China, Taiyuan 030008, China
[d] School of Materials Science and Engineering, National Engineering Research Center for Advanced Polymer Processing Technology, Zhengzhou University, Zhengzhou 450002, Henan, China
[e] Integrated Composites Laboratory (ICL), Department of Chemical & Biomolecular Engineering, University of Tennessee, Knoxville, TN 37996, USA
[f] School of Material Science and Engineering, Jiangsu University of Science and Technology (JUST), Zhenjiang, Jiangsu, 212003, China
[g] State Key Laboratory of Marine Resource Utilization in South China Sea, Hainan University, Haikou 570228, China
[h] College of Materials Science and Engineering, Shandong University of Science and Technology, Qingdao 266590, China

ARTICLE INFO

Article history:
Received 29 January 2018
Received in revised form
8 April 2018
Accepted 20 April 2018
Available online 25 April 2018

Keywords:
Nb metal
Doping
Lattice deformation
Hydrogen-diffusion coefficient (DH)
Mechanical property

ABSTRACT

The structures and mechanical properties of Nb-Mo-Co(Ru) solid solutions for hydrogen permeation have been investigated by X-ray diffraction (XRD) analysis, pressure-composition-temperature (PCT) measurements, and three-point bending tests. The as-prepared $Nb_{86}Mo_{14}$, $Nb_{86}Mo_7Co_7$, and $Nb_{86}Mo_7Ru_7$ samples composed of Nb-based solid solutions with bcc structures were hydrogenated into their corresponding hydrides to give the $NbH_{0.95}$ phases after hydrotreatment. The largest lattice deformations of the bcc structure and $NbH_{0.95}$ phase were observed in the $Nb_{86}Mo_7Ru_7$ sample. This sample possessed the highest hydrogen-diffusion coefficient value (2.32×10^{-9} cm/s), the lowest hydride formation enthalpy (−21.4 kJ/(mol·H_2)), and the maximum force before and after hydrogenation. Overall, these results demonstrate that the addition of Ru improves hydrogen diffusion and enhances the mechanical properties of $Nb_{86}Mo_{14}$ alloy against hydrogen embrittlement.

1. Introduction

Membrane reactors that employ dense hydrogen separation and purification alloys are one of the most important components for industrial hydrogen production by the steam reforming of natural gas [1–3]. Recently, the increased demand of ultra-pure hydrogen for various applications like anode reactants of fuel cells, semiconductor fabrication, foodstuff hydrogenation, and production of high-purity chemical feedstock has intensified the metal membrane research [4–6]. Polymer materials have potential to store hydrogen while at low temperatures [7,8]. Pd and its alloys are now widely used for hydrogen separation and purification; the obvious disadvantage of these relatively rare alloys is their high cost. In this respect, Group 5 metals (i.e., vanadium (V), niobium (Nb), and tantalum (Ta)) have generated considerable interests as promising hydrogen separation materials due to their lower price and higher hydrogen permeability than the currently used Pd-based alloys [9–12]. However, their poor resistance to hydrogen embrittlement poses a significant barrier to their practical use [9,10,13,14].

Experimental studies have verified that alloying of metals is an effective way to address this problem [12–15]. Recent theoretical studies by Watanabe et al. have shown that the addition of W could decrease the hydrogen solubility in Nb and therefore improve its resistance to hydrogen embrittlement [12,16]. In addition, Hu et al. found that the addition of W can increase the mechanical properties of $Nb_{16}H$ phases, decrease the structural stability of the

* Corresponding author.
** Corresponding author.
*** Corresponding author.
E-mail addresses: houmaliufei999@163.com (F. Liu), zmwang@guet.edu.cn (Z. Wang), zguo10@utk.edu (Z. Guo).

https://doi.org/10.1016/j.jallcom.2018.04.235
0925-8388/

$Nb_{15}WH$ (T) phase, and lower the diffusion barrier for H while enhance its diffusion paths [17]. Both W and Mo are high-Z refractory metals with similar physical properties. Compared with W, however, Mo is a superior alloying candidate for Nb-based alloy membranes for hydrogen permeation because of its unique properties, including a lower melting point (2883 K), lower erosion rate, higher diffusivity, and lower solubility of H in Mo, which lead to a lower H retention [18–20]. In our previous work, the effects of Mo alloying on the structural stability, H diffusion, and mechanical properties of the NbH phase were investigated by first-principles DFT calculations; four Mo atoms were necessary to reach the equivalent of an experimental composition of 25 at.% Mo in NbH [12,13,16,21]. The calculated results revealed that such a configuration leads to a lower energy barrier for H diffusion, a higher diffusion coefficient (D_H), and improved mechanical properties of the Nb metal. Additional experimental studies indicated that $Nb_{86}Mo_{14}$ has a higher D_H value, higher hydride formation enthalpy, and maximum force and displacement before and after hydrogenation. Overall, these results indicate that alloying Nb with Mo can improve the hydrogen-diffusion behavior and anti-bending properties of Nb metal.

In this paper, Co and Ru were used as secondary doping elements to replace half of the Mo atoms in $Nb_{86}Mo_{14}$. The effects of this type of double-element doping on the phase structure, H-diffusion coefficient, and mechanical properties of $Nb_{86}Mo_{14}$ solid solutions were then investigated. The results show that the addition of Ru improves the hydrogen diffusion and enhances the mechanical properties of $Nb_{86}Mo_{14}$ alloy against the hydrogen embrittlement.

2. Experimental details

2.1. Preparation and structural characterization of Nb-Mo-Co(Ru) alloy samples

Nb (99.99% purity), Mo (99.99% purity), Co (99.99% purity), and Ru (99.99% purity) were used as the starting materials. Cobalt is very hard and brittle, and it can enhance the strength of niobium which has good ductility and hydrogen permeability. Molybdenum has high strength, hardness, solderability and toughness. It is often used as an additive for alloy and stainless steel. Ingots with nominal compositions of $Nb_{86}Mo_{14}$, $Nb_{86}Mo_7$ Co_7, and $Nb_{86}Mo_7Ru_7$ alloys were produced by a melting method in a KW-II non-consumable electrode induction melting furnace (Beijing BOE Optoelectronics Technology Co., Ltd.). The ingots were annealed at 1273 K for 96 h under vacuum (10^{-3} Pa) to obtain a uniform structure and composition, after which they were quenched in ice water before use. X-ray diffraction (XRD) analysis of the samples was performed on an Empyrean PIXcel 3D (PANalytical B.V., Holland, Cu K_α radiation) diffractometer. The collected XRD data were then evaluated using the Rietveld profile refinement method with the FULLPROF software package. Fractographic analysis of the alloy membranes was performed using a Quanta450FEG/X-Max20 (SEM/EDS, FEI, USA).

2.2. Measurement of PCT curves and hydrogen diffusion coefficient (D_H)

The pressure-composition-temperature (PCT) curves of the sample powders (~0.5 g, ≥200 mesh) at different temperatures (573, 613, and 653 K) were measured using a Sievert-type apparatus (Setaram PCTPro-2000). Before testing, three absorbing-desorbing cycles were necessary to fully activate the samples. The activation conditions were set at 673 K under 2 MPa of hydrogen pressure.

The hydrogen diffusion behavior of the alloy samples was studied by a potentiostatic method using a Solartron SI1287 potentiostat at a 100% charge state with a potential step and discharge time of +500 mV and 3600 s, respectively. The hydrogen diffusion coefficient (D_H) can be evaluated according to Eq. (1) [23]:

$$\log i = \log\left[\pm\frac{6FD}{da^2}(C_0 - C_S)\right] - \left(\frac{\pi^2}{2.303}\right)\left(\frac{D}{a^2}\right)t \quad (1)$$

where i represents the diffusion current density (mA/g); F is the Faraday constant; D is the hydrogen-diffusion coefficient (cm^2/s); d is the powder density (g/cm^3); a is the alloy particle radius of the powder (cm), for which an average value of 50 μm was used for the alloy powder sieved by 200 standard screening; C_0 is the initial hydrogen concentration (mol/cm^3); C is the hydrogen concentration at the particle surface (mol/cm^3); and t is the discharge time (s). Given Eq. (1), it is clear that the value of D can be derived from the slope of $logi$–t curves. Before testing, the alloy electrodes were prepared by mixing the alloy powders with carbonyl nickel powders at a weight ratio of 1:3 and then cold pressed into a pellet under 10 MPa.

The electrochemical studies were performed in a half-cell consisting of a working electrode, a sintered $Ni(OH)_2$/NiOOH counter electrode, and a Hg/HgO reference electrode. The electrolyte was a 6 M KOH solution.

2.3. Mechanical performance of the metallic membranes

A three-point bending test was conducted to measure the bending stress of the alloy membranes of size $L_s \times b \times h = 18\ mm \times 6\ mm \times 0.8\ mm$. When the membranes were in the elastic range, the maximum bending stress is σ ($\sigma = M/W$); here, $M = FLs/4$, $W = (bh^2)/6$ [22,23], F is the bending force, L_s is the span length, and b and h are the width and thickness of the membrane sample, respectively. Detailed information of this test is provided in the literature [24,25].

3. Results and discussion

3.1. Structure of Nb-Mo-Co(Ru) alloy samples before and after hydrogenation

Refined XRD data of the as-prepared $Nb_{86}Mo_{14}$, $Nb_{86}Mo_7Co_7$, and $Nb_{86}Mo_7Ru_7$ alloy samples are shown in Fig. 1, where the red

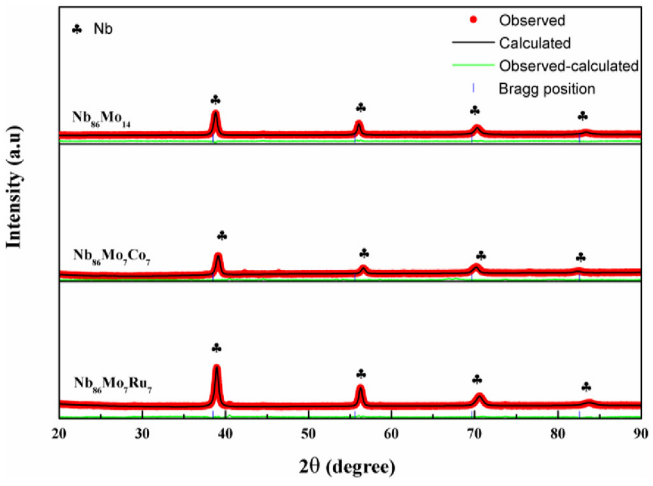

Fig. 1. XRD patterns of the as-melted Nb-Mo-Co(Ru) alloy samples.

Table 1
Calculated lattice parameters of Nb-Mo-Co(Ru) solid solutions with BCC structures.

Formula	a (Å)	b (Å)	c (Å)	V (Å^3)
Nb(ICSD89-5157)	3.300	3.300	3.300	35.973
$NbH_{0.95}$(ICSD80-2282)	3.447	4.860	4.860	81.417
As-Prepared$Nb_{86}Mo_{14}$	3.2765(3) (0.71%)*	3.2765(3) (0.71%)*	3.2765(3) (0.71%)*	35.175(7) (2.22%)*
$Nb_{86}Mo_{14}$hydride	3.4003(0) (1.35%)*	4.8154(9) (0.92%)*	4.7798(0) (1.65%)*	78.265(0) (3.87%)*
As-Prepared$Nb_{86}Mo_7Co_7$	3.2382(3) (1.87%)*	3.2382(3) (1.87%)*	3.2382(3) (1.87%)*	33.956(5) (5.61%)*
$Nb_{86}Mo_7Co_7$hydride	3.3583(2) (2.57%)*	4.7613(0) (2.03%)*	4.6847(0) (3.61%)*	74.908(2) (7.99%)*
As-Prepared$Nb_{86}Mo_7Ru_7$	3.2761(6) (0.72%)*	3.2761(6) (0.72%)*	3.2761(6) (0.72%)*	35.163(7) (2.25%)*
$Nb_{86}Mo_7Ru_7$ hydride	3.3716(1) (2.18%)*	4.7840(9) (1.63%)*	4.7413(8) (2.44%)*	76.478(8) (6.06%)*

Note: the data marked with "*" is the calculated variation of the lattice parameters relative to ICSD reference data.

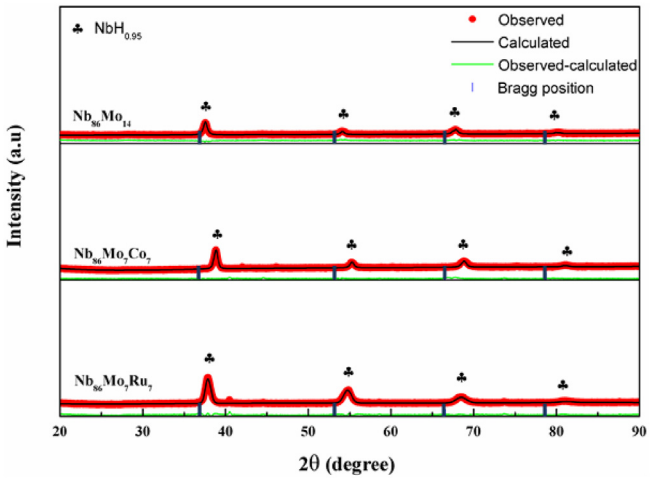

Fig. 2. XRD patterns of Nb-Mo-Co(Ru) alloy samples after hydrogenation treatment.

and black lines correspond to the experimentally observed and calculated patterns, respectively.

The blue lines indicate the standard patterns, whereas the green lines represent the difference between the observed and calculated patterns. The as-prepared Nb-Mo-Co(Ru) samples are composed entirely of Nb-based solid solutions with a body-centered cubic (bcc) structure, and no new phase is formed. The calculated lattice parameters of these samples are listed in Table 1. Compared with pure Nb, clear lattice deformations can be observed for these Nb-Mo-Co(Ru) alloy samples owing to different atomic sizes of Nb (1.429 Å), Mo (1.362 Å), Co (1.253 Å), and Ru (1.325 Å). Fig. 2 and Table 2 show the refined XRD data of the $Nb_{86}Mo_{14}$, $Nb_{86}Mo_7Co_7$, and $Nb_{86}Mo_7Ru_7$ alloy samples after hydrogenation.

The results indicate that these solid solutions are hydrogenated into their corresponding hydrides with the $NbH_{0.95}$ phase after hydrotreatment under 2 MPa of hydrogen pressure at 653 K. Similar changes in the lattice parameters have also been detected in the hydride samples. Based on the structure analysis before and after hydrogenation, it is suggested that the as-prepared alloys are all Nb-based solid solutions with bcc structures, which can be hydrogenated into Nb-based hydrides with $NbH_{0.95}$ phases after hydrotreatment. Partial replacement of Nb does not lead to the formation of a new phase, but instead results in the lattice deformation due to different atomic sizes of Nb and the dopants. A larger variation in lattice parameters was observed for the $Nb_{86}Mo_7Ru_7$ sample and its corresponding hydride; the degree of variation of the lattice parameters (a, b, c, V) for the bcc structure is 2.57% for a, 2.03% for b, 3.61% for c, and 7.99% for V, and that of the $NbH_{0.95}$ phase is 2.18%, 1.63%, 2.44%, 6.06%, respectively, as shown in Table 1.

3.2. Hydrogenation performance of Nb-Mo-Co(Ru) powder samples

To evaluate the structural stability of the Nb-based hydrides, the hydride formation enthalpy (ΔH) has been derived from the PCT analysis [26–28]. The PCT curves at three temperatures (573, 613, and 653 K) are shown in Fig. 3(a–c). As seen, the hydriding platform pressure increases with increasing the temperature. The formation enthalpies of the Nb-based hydrides have been calculated using the van't-Hoff equation. As seen in Fig. 3(d), a good linear relation between $\ln P_{eq}$ and (1/T) with a slope of ΔH/R is observed for all three samples. The calculated hydride formation enthalpies (ΔH) are −35.8 kJ/(mol·H_2) for $Nb_{86}Mo_{14}$, −30.6 kJ/(mol·H_2) for $Nb_{86}Mo_7Co_7$, and −21.4 kJ/(mol·H_2) for $Nb_{86}Mo_7Ru_7$. Note that a larger absolute value of ΔH is indicative of a higher stability. The addition of Ru reduces the enthalpy value, which is conducive to the absorption of hydrogen. Thus, the results imply that replacing half of the Mo atom with Ru in $Nb_{86}Mo_{14}$ improves the dehydrogenation behavior and hydrogen-permeable ability of the Nb-based solid solution.

3.3. Measurement of hydrogen diffusion coefficient (D_H)

Fig. 4 shows the relationship curves of the hydrogen permeability current density and time, as measured by the potentiostatic method. Based on the spherical electrode diffusion theory, the hydrogen diffusion coefficient (D_H) can be calculated from the slope of the log$i$–t curves. This approach gives the calculated D_H values of 1.84×10^{-9} cm/s for $Nb_{86}Mo_{14}$, 0.68×10^{-9} cm/s for $Nb_{86}Mo_7Co_7$, and 2.32×10^{-9} cm/s for $Nb_{86}Mo_7Ru_7$. These results suggest that the addition of Ru leads to an improvement of the hydrogen diffusion behavior of the $Nb_{86}Mo_{14}$ sample, which can be attributed to the larger lattice deformation and higher formation enthalpy of the corresponding hydride in $Nb_{86}Mo_7Ru_7$. Similar work has been reported by Iwakura et al. using $aMnNi_{4.0-x}Mn_{0.75}Al_{0.25}Co_x$ alloy sample [29,30]. In that case, hydrogen diffusion in the a-phase was diminished as the cobalt content increased because of the strong attractive interactions between the absorbed hydrogen atoms,

Table 2
Data of three-point bending test of the Nb-Mo-Co(Ru) alloy membranes before and after hydrogenation.

Alloy number	N1	N2	N3	N4	N5	N6
Maximum force, F (N)	91.3080	99.9593	113.8878	17.4411	21.6929	22.7722
Maximum displacement, L (mm)	0.44902	0.5030	0.4740	0.1844	0.2022	0.1835

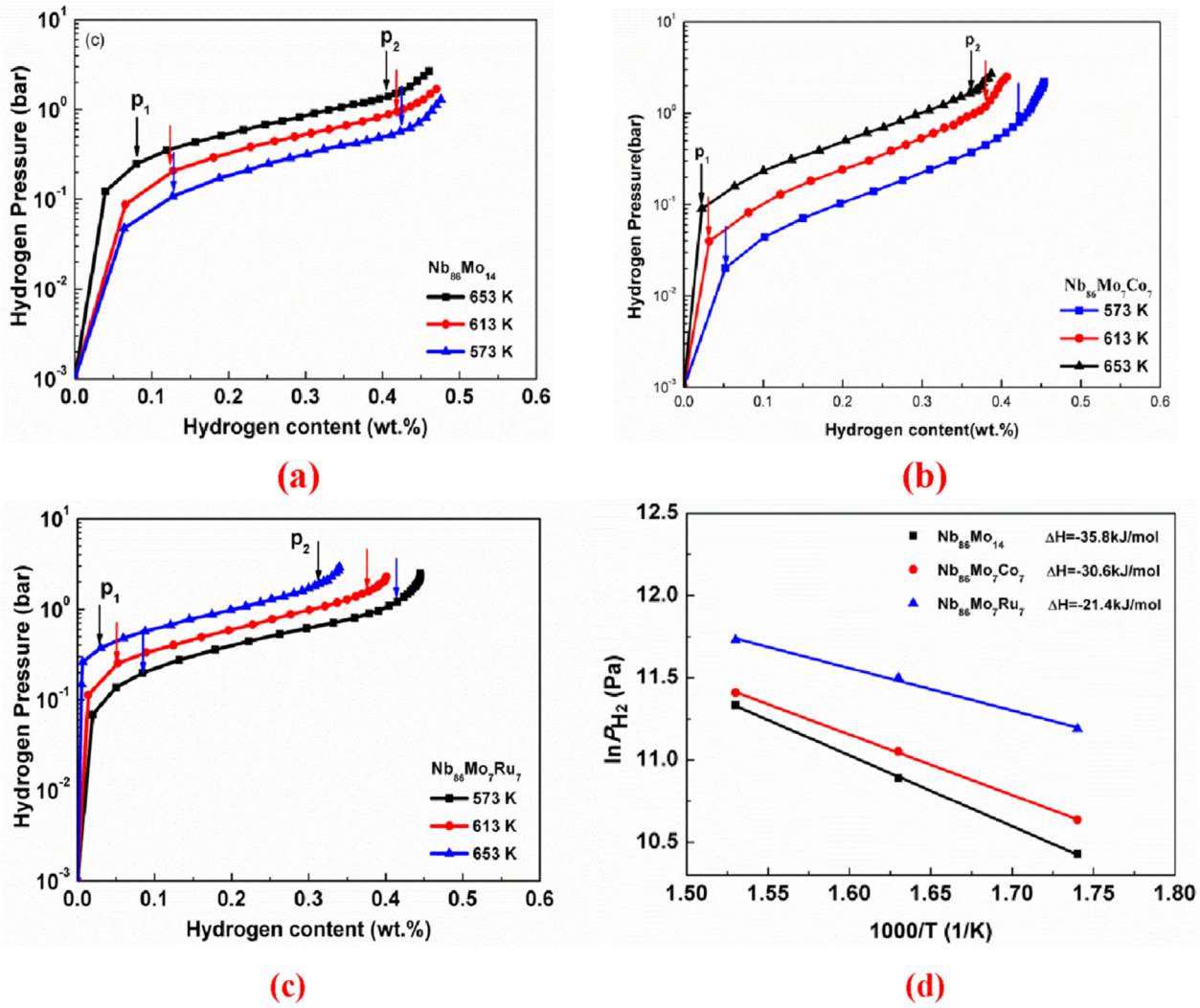

Fig. 3. Hydrogen absorption curves and the derived hydride-formation enthalpies of Nb-Mo-Co(Ru) alloy samples.

which is caused by its large lattice deformation. However, further work is required to elucidate the underlying mechanism of this process.

3.4. Mechanical properties of Nb-Mo-Co(Ru) alloy membranes before and after hydrogenation

The mechanical properties of the Nb-Mo-Co(Ru) alloy membranes were determined using the three-point bending test as shown in Fig. 5. The results are shown in Fig. 6 and Table 2. The pristine Nb-Mo-Co(Ru) alloy membranes exhibited better mechanical properties than the corresponding hydrogenation-treated samples. The maximum force and maximum displacement of the pristine $Nb_{86}Mo_7Ru_7$ sample are 113.8878 N and 0.5030 mm, respectively. In contrast, poor mechanical properties were observed for the hydrogenation-treated Nb-Mo-Co(Ru) samples. Such a clear reduction in the mechanical property performance can be attributed to hydrogen embrittlement resulting from the hydrotreatment. However, regardless of whether or not hydrogenation treatment was performed, both the maximum force and maximum

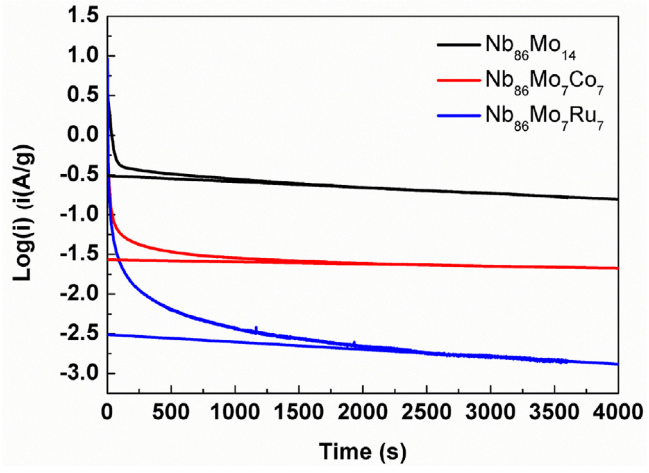

Fig. 4. Hydrogen permeation curves of Nb-Mo-Co(Ru) alloy samples measured by a potentiostatic method.

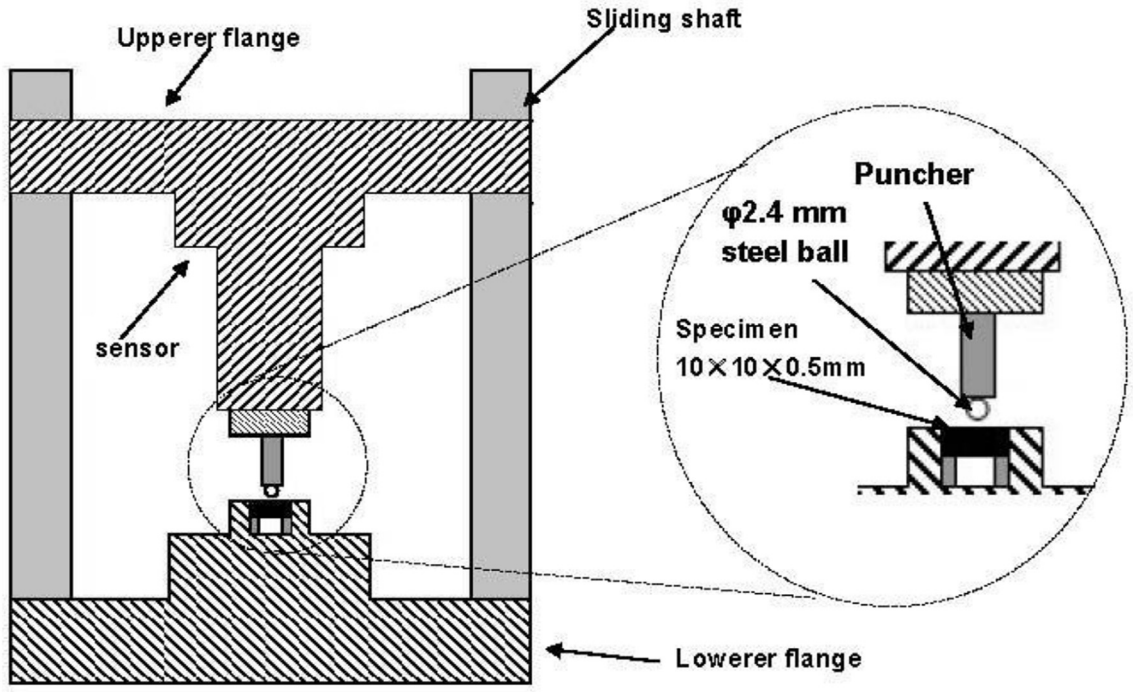

Fig. 5. Mechanical properties test schematic of hydrogen separation alloy films.

displacement increased in these two double-element doping samples, indicating that the addition of Ru (or Co) can improve the mechanical properties of $Nb_{86}Mo_{14}$ sample.

Generally, there exists a strong affinity between hydrogen and Groups 4 and 5 elements. The produced brittle hydride after hydrogenation may possibly lead to cracks and their enlargement, resulting in a reduced plasticity or strength of the materials that may not be recoverable. In order to verify the results of the three-point bending test, SEM fractographic analysis of the above-mentioned Nb-Mo-Co(Ru) samples before and after hydrogenation was performed. The corresponding SEM images are shown in Fig. 7. Relative to the pristine Nb-Mo-Co(Ru) membrane samples, obvious hydrogen embrittlement cracks can be observed in the samples after hydrogenation, especially in $Nb_{86}Mo_{14}$. As can be seen from N5 and N6, the cracks decreased obviously after hydrogen percolation because of the addition of Co and Ru respectively, which effectively suppressed the problem of hydrogen embrittlement, and the addition of Ru was more significant. These results can be attributed to the larger lattice deformation of $Nb_{86}Mo_7Ru_7$ due to different atomic sizes of Nb and the dopants. Similar results have also been reported for Mo [23–25], W [23], and Nb [26] metals.

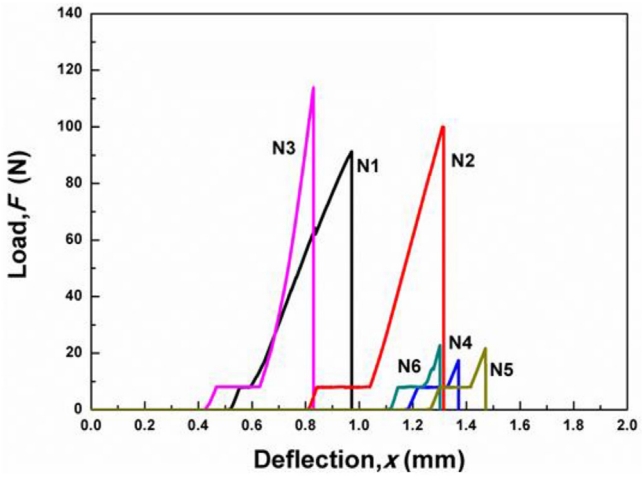

Fig. 6. Three-point bending curves of Nb-Mo-Co(Ru) alloy membranes before/after hydrogenation. N1: Pristine $Nb_{86}Mo_{14}$, N2: Pristine $Nb_{86}Mo_7Co_7$, N3: Pristine $Nb_{86}Mo_7Ru_7$, N4: $Nb_{86}Mo_{14}$ sample after hydrogenation, N5: $Nb_{86}Mo_7Co_7$ sample after hydrogenation, N6: $Nb_{86}Mo_7Ru_7$ sample after hydrogenation.

4. Conclusions

In this study, the as-prepared $Nb_{86}Mo_{14}$, $Nb_{86}Mo_7Co_7$, and $Nb_{86}Mo_7Ru_7$ alloy samples composed of Nb-based solid solutions with bcc structures were hydrogenated into their corresponding hydrides with $NbH_{0.95}$ phases after hydrotreatment. Doping treatment leads to the lattice deformations of both the bcc structure and the $NbH_{0.95}$ phase due to atomic size differences between Nb and the dopant atoms (Mo, Co, and Ru). The largest lattice deformation is observed for the $Nb_{86}Mo_7Ru_7$ sample and its hydride. Specifically, the $Nb_{86}Mo_7Ru_7$ sample has the highest D_H value (2.32×10^{-9} cm/s), lowest hydride-formation enthalpy ($\triangle H = -21.4$ kJ/(mol·H_2)), and the maximum force before and after hydrogenation (113.8878 N and 22.7722 N, respectively). Overall, these results indicate that the addition of Ru will improve hydrogen diffusion and enhance the mechanical properties of $Nb_{86}Mo_{14}$ alloy against hydrogen embrittlement.

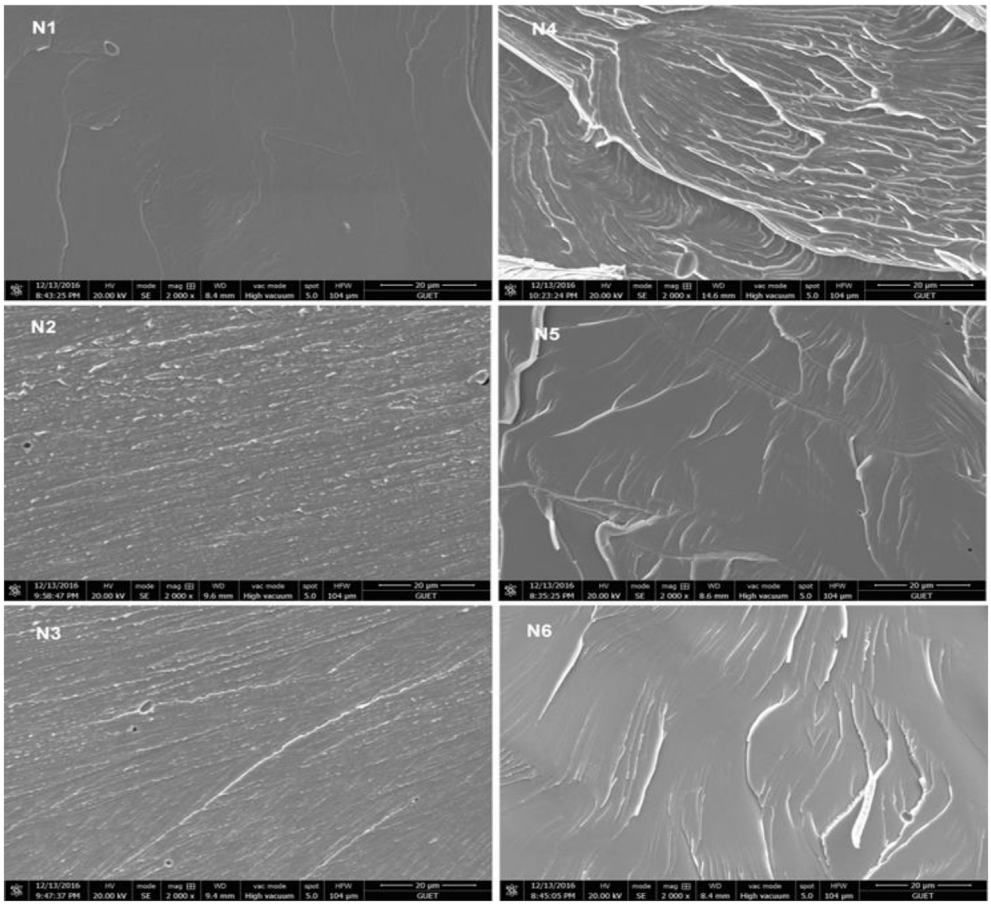

Fig. 7. SEM fractographic images of Nb-Mo-Co(Ru) alloy membranes before/after hydrogenation. N1: Pristine $Nb_{86}Mo_{14}$, N2: Pristine $Nb_{86}Mo_7Co_7$, N3: Pristine $Nb_{86}Mo_7Ru_7$, N4: $Nb_{86}Mo_{14}$ sample after hydrogenation, N5: $Nb_{86}Mo_7Co_7$ sample after hydrogenation, N6: $Nb_{86}Mo_7Ru_7$ sample after hydrogenation.

Acknowledgements

This work was financially supported by the National Natural Science Foundation of China (51471055), the Program for Post-graduate Joint Training Base of GUET-CJYRE(No.20160513-20-Z), the Science and Technology Innovation Team Project of Guangxi Province (2016GXNSFGA380001), Sponsored by the Fund for Key supports funding projects for Discipline Construction of Shanxi province (Jinjiao research [2015]10), the Leader of the youth discipline of Taiyuan Institute of Technology, Shanxi "1331 Project" Collaborative Innovation Center.

References

[1] E. Kikuchi, Membrane reactor application to hydrogen production, Catal. Today 56 (2000) 97–101.
[2] S. Pati, R.A. Jat, N.S. Anand, Pd-Ag-Cu dense metallic membrane for hydrogen isotope purification and recovery at low pressures, J. Membr. Sci. 522 (2017) 151–158.
[3] Z. Sun, et al., Experimental and simulation understanding of morphology controlled barium titanate nanoparticles under co-adsorption of surfactants, CrystEngComm 19 (2017) 3288–3298.
[4] S. Pati, R.A. Jat, N.S. Anand, Pd-Ag-Cu dense metallic membrane for hydrogen isotope purification and recovery at low pressures, J. Membr. Sci. 522 (2017) 151–158.
[5] C. Wang, B. Mo, Z. He, C.X. Zhao, L. Zhang, Q. Shao, X. Guo, E. Eujcik, Z. Guo, Hydroxide ions transportation in polynorbornene anion exchange membrane, Polymer 138 (2018) 363–368.
[6] X. Cheng, Z. Wang, X. Jiang, et al., Towards sustainable ultrafast molecular-separation membranes: from conventional polymers to emerging materials, Prog. Mater. Sci. 92 (2018) 258–283.
[7] X. Jiang, S.w. Li, L. Shao, Pushing CO_2-philic membrane performance to the limit by designing semi-interpenetrating networks (SIPN) for sustainable CO_2 separations, Energy Environ. Sci. 10 (2017) 1339.
[8] X.B. Yang, Z.X. Wang, L.S, Construction of oil-unidirectional membrane for integrated oil collection with lossless transportation and oil-in-water emulsion purification, J. Membr. Sci. 549 (2018) 67.
[9] R. Ramachandran, R.K. Menon, An overview of industrial uses of hydrogen, Int. J. Hydrogen Energy 23 (1998) 593–598.
[10] S.C. Chen, C.C.Y. Hung, G.C. Tu, Perturbed hydrogen permeation of a hydrogen mixture-New phenomena in hydrogen permeation by Pd membrane, Int. J. Hydrogen Energy 33 (2008) 1880–1889.
[11] S.N. Paglieri, J.D. Way, Innovations in palladium membrane research, Separ. Purif. Meth. 31 (2002) 1–169.
[12] A. Suzuki, H. Yukawa, T. Nambu, Analysis of pressur-e–composition–isotherms for design of non-Pd-based alloy membranes with high hydrogen permeability and strong resistance to hydrogen embrittle-ment, J. Membr. Sci. 503 (2016) 110–115.
[13] N. Watanabe, H. Yukawa, T. Nambu, Alloying effects of Ru and W on the resistance to hydrogen embrittlement and hydrogen permeability of niobium, J. Alloys Compd. 477 (2009) 851–854.
[14] G.X. Zhang, H. Yukawa, T. Nambu, Alloying effects of Ru and W on hydrogen diffusivity during hydrogen permeation through Nb-based hydrogen perme-able membranes, Int. J. Hydrogen Energy 35 (2010) 1245–1249.
[15] J.R. Slining, D.A. Koss, Solid solution strengthening of high purity niobium alloys, Metall. Mater. Trans. B 4 (1973) 1261–1264.
[16] S. Kozhakhmetov, N. Sidorov, V. Piven, Alloys based on group 5 metals for hydrogen purification membranes, J. Alloys Compd. 645 (2015) S36–S40.
[17] H. Yukawa, T. Nambu, Y. Matsumoto, Alloy design of Nb-based hydrogen permeable membrane with strong resistance to hydrogen embrittlement, Mater. Trans. 49 (2008) 2202–2207.
[18] Y.T. Hu, H. Gong, L. Chen, Fundamental effects of W alloying on various properties of NbH phases, Int. J. Hydrogen Energy 40 (2015) 12745–12749.
[19] S. Nagata, K. Takahiro, Deuterium retention in tungsten and molybdenum, J. Nucl. Mater. 283 (2000) 1038–1042.
[20] C. Duan, Y.L. Liu, H.B. Zhou, First-principles study on dissolution and diffusion properties of hydrogen in molybdenum, J. Nucl. Mater. 404 (2010), 109–115.5.

[21] G.M. Wright, D.G. Whyte, B. Lipschultz, Measurement of hydrogenic retention and release in molybdenum with the DIONISOS experiment, J. Nucl. Mater. 390 (2009) 544–549.
[22] H. Yukawa, G.X. Zhang, N. Watanabe, Analysis of hydrogen diffusion coefficient during hydrogen permeation through niobium and its alloys, J. Alloys Compd. 476 (2009) 102–106.
[23] G. Sandrock, A panoramic overview of hydrogen storage alloys from a gas reaction point of view, J. alloys compd. 293 (1999) 877–888.
[24] H.G. Zhang, Z.M. Wang, F. Liu, Mechanical properties of Nb-Ti-Ni alloy membranes for hydrogen permeation, Rare Metal Mater. Eng. 45 (2016) 1443–1448.
[25] Y. Ushiro, D. Okai, A. Yamamoto, In situ observation of fracture behavior of CrN/Cr film during three-point bending test, Adv. Mater. Res. 922 (2014) 779–784.
[26] A. Nespoli, E. Villa, L. Bergo, DSC and three-point bending test for the study of the thermo-mechanical history of NiTi and NiTi-based orthodontic archwires, J. Therm. Anal. Calorim. 120 (2015) 1129–1138.
[27] Y.Q. Ren, H.Y. Zeng, Z.Y. Wang, Application of high pressure gas adsorption instrument Pro PCT in the research and development of hydrogen storage materials, Mater. Sci. Techn. Equip. China (2011) 4–6 (in Chinese).
[28] K.C. Chou, K. Xu, A new model for hydriding and dehydriding reactions in intermetallics, Intermetallics 15 (2007) 767–777.
[29] L.Z. Ouyang, X.S. Yang, H.W. Dong, Structure and hydrogen storage properties of Mg_3Pr and $Mg_3PrNi_{0.1}$ alloys, Scr. Mater. 61 (2009) 339–342.
[30] C. Iwakura, K. Fukuda, H. Senoh, Electrochemical characterization of $MmNi_{4.0-x}Mn_{0.75}Al_{0.25}Co_x$ electrodes as a function of cobalt content, Electrochim. Acta 43 (1998) 2041–2046.